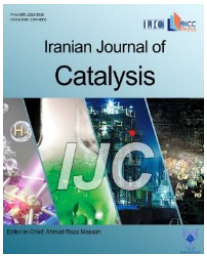

Iran. J. Catal. 2026; 16(1): 127-140

Iranian Journal of Catalysis (IJC)

https://doi.org/10.57647/ijc.2026.1601.08

Research Article

Linking Quantum Chemistry and Electrochemistry: Interfacial ORR Mediated by Tetracyanoquinodimethane (TCNQ) and Proton Shuttle Di-pyridinamine (DPA)

Fatemeh Soleymani-Bonoti*

Department of Chemistry, Faculty of Science, Jundi-Shapur University of Technology, Dezful, Iran

*Corresponding authors: soleymani.86@gmail.com

Article History:

Received:
11 September 2025

Revised:
9 December 2025

Accepted:
18 December 2025

Published Online:
24 December 2025

Published in Issue:
31 March 2026

Abstract

This study investigates the oxygen reduction reaction (ORR) at the water 1,2-dichloroethane (DCE) interface using tetracyanoquinodimethane (TCNQ) as an electron mediator and 2,2-dipyridylamine (DPA) as a proton shuttle, combining electrochemical measurements with Hartree-Fock and DFT calculations. TCNQ facilitates interfacial electron transfer, exhibiting reversible stepwise reductions ($TCNQ/TCNQ^{-}/TCNQ^{2-}$) with rate constants of ~7×10^{-3} to 1.5×10^{-1} cm s^{-1}, while quantum chemical analysis reveals its modest proton affinity (PA ~16–95 kJ mol^{-1} for mono-protonated form) and weak aqueous basicity (pK_a >12), confirming its primary role in electron mediation rather than protonation. DPA addition (2.4–5.6 $\times10^{-6}$ M) enhances cathodic/anodic peak currents in cyclic voltammetry, enabling proton-coupled electron transfer (PCET) that boosts H_2O_2 yield from 38% (4 mM) (TCNQ alone) to 78% (8 mM) via synergistic proton relay, as validated by iodometric assays and a proposed mechanism involving $O_2 \rightarrow O_2^{-} \rightarrow HO_2$. These findings highlight a cooperative molecular relay at soft interfaces, offering design principles for efficient biphasic electrocatalysts in energy applications.

Keywords: Liquid–Liquid Interface (ITIES); Oxygen Reduction Reaction (ORR); Proton-Coupled Electron Transfer (PCET); Proton Affinity (PA); Tetracyanoquinodimethane (TCNQ)

Cite this article: F. Soleymani-Bonoti, Iran. J. Catal. **16** (2026) 127-140. https://doi.org/10.57647/ijc.2026.1601.08

1. Introduction

The reduction of molecular oxygen (O_2) is a fundamental reaction in many electrochemical and biological processes, including fuel cells, enzymatic respiration, and oxidative catalysis [1-5]. While the oxygen reduction reaction (ORR) has traditionally been studied at solid electrodes in homogeneous media [6, 7]. Recent advances have highlighted the potential of conducting the ORR at the interface between two immiscible electrolyte solutions (ITIES), typically composed of an aqueous and an organic phase. This interface provides a unique soft and polarized environment where aqueous protons and organic electron donors can combine to reduce O_2, enabling proton-coupled electron transfer reactions. Studies have shown that ORR at ITIES mimics biological soft interfaces, such as biomembranes, offering a novel approach for interfacial catalysis with electrochemical control through the applied potential difference across the two phases. [8-10]. Such soft interfaces present a unique environment for exploring redox catalysis beyond conventional solid–liquid boundaries. At the interface between two immiscible electrolyte solutions (ITIES), interfacial electron transfer occurs between redox-active species dissolved in separate phases. However, while significant efforts have focused on enhancing electron transfer at

these interfaces, the equally crucial step of proton transfer has received comparatively less attention. The complete reduction of oxygen to hydrogen peroxide (H_2O_2) or water (H_2O) requires a carefully balanced delivery of electrons and protons in the correct stoichiometry and timing. Proton-coupled electron transfer (PCET) is fundamental to this process, where the rates of proton and electron transfer must be synchronized to minimize undesired side products and maximize selectivity to water. A mismatch in these rates can lead to partial reduction products such as hydrogen peroxide or superoxide, while well-coordinated proton flux ensures efficient water formation [9, 11, 12]. In biphasic systems, this balance is disrupted by the proton-deficient nature of the organic phase, making proton transport a common rate-limiting step [9]. To address the limitation in proton transfer at ITIES during ORR, proton shuttles or transfer catalysts can be employed. Often these are amphiphilic acids, π-conjugated systems, or nitrogen-containing bases that preferentially accumulate at the interface.

These molecules facilitate proton migration from the aqueous phase into the interfacial region where ORR occurs, thus enhancing proton delivery. Such proton relays or shuttles play a critical role in synchronizing proton and electron transfer rates, improving overall ORR efficiency. For example, nitrogen-containing groups positioned near active catalytic sites can serve as proton relays, accelerating proton transfer kinetics and stabilizing key reaction intermediates during ORR. This coordinated proton shuttle mechanism helps overcome kinetic bottlenecks and enhances selectivity for water formation over partial reduction products. [9, 11, 13-15]. Proton shuttles facilitate proton transfer and significantly influence the kinetics and selectivity of the ORR. They direct the reaction toward either the two-electron pathway producing H_2O_2 or the four-electron pathway generating H_2O. This selectivity depends largely on the shuttles' ability to stabilize intermediates through hydrogen bonding and electronic delocalization [16-19]. Therefore, designing effective interfacial catalysts requires a deep understanding of PCET mechanisms within complex solvation and redox environments. Optimizing PCET at the ITIES is crucial for enhancing catalytic activity and selectivity in biphasic systems [3, 8, 10, 12, 20].

Recent advances in interfacial electrocatalysis, biomimetic proton shuttles, and molecular mediators for the oxygen reduction reaction (ORR) have significantly enriched the scientific understanding in this area. Notably, proton-coupled electron transfer (PCET) processes at liquid–liquid interfaces have been explored in studies by MU Khan et al. and S. Sarfraz et al. [21, 22], which provide important mechanistic insights relevant to biphasic electrochemical systems. Biomimetic catalysts for oxygen reduction, as reported by S. Naz et al., [23] Highlight molecular design strategies that inspire the development of effective electrocatalysts.

Furthermore, the role of redox mediators in molecular electrocatalysis has been extensively studied by MRSA Janjua et al. [24] and S. Shahzadi et al., [25] emphasizing their impact on enhancing electron transfer processes. Complementing these findings, recent work on synthetic proton relays and organic electron acceptors by MRSA Janjua [26, 27], T. Mubashir et al., [28] and B. Basha et al [29]. provides a crucial understanding of proton transport and electron acceptance mechanisms, which are fundamental for improving interfacial electrocatalytic performance. Incorporating these broader perspectives strengthens the scientific foundation and contextualizes the present study within the rapidly evolving field. These systems offer significant potential for clean energy technologies and green chemical processes, especially in applications where solid electrodes are undesirable or impractical among the key descriptors of a molecule's ability to mediate proton transport are its proton affinity (PA) and gas-phase basicity (GB).

These thermodynamic parameters reflect the molecule's intrinsic capacity to accept and stabilize protons, offering critical insights into the feasibility and directionality of interfacial PCET [3, 9, 11-13]. Molecules with appropriately tuned proton affinity (PA) and gas-phase basicity (GB) can serve as dynamic proton relays, improving proton delivery across the nonpolar phase and promoting efficient multi-electron oxygen reduction.

In this context, quantum chemical calculations have become powerful tools for predicting PA, GB, and aqueous pKa values when direct experimental measurements of interfacial protonation equilibria are not available.

These computational insights enable the rational design of redox-active mediators and proton shuttles that work synergistically in biphasic oxygen reduction reaction (ORR) environments [9, 11].

Accurate modeling of these parameters is therefore not only theoretical but also essential for the engineering of supramolecular electrocatalytic systems at soft interfaces. In this study, we investigate the role of tetracyanoquinodimethane (TCNQ) as a redox mediator capable of participating in PCET at ITIES, with catalytic support from 2,2′-dipyridylamine (DPA) serving as a proton shuttle.

Using density functional theory (DFT), we calculated the proton affinity, gas-phase basicity, and pKa of TCNQ and its reduced forms to evaluate their ability to stabilize protons via the cyano groups.

These computational results are combined with electrochemical experiments to provide a molecular-level understanding of how TCNQ and DPA cooperatively facilitate proton–electron coupling in the ORR across soft liquid–liquid interfaces.

10.57647/ijc.2026.1601.08

Our findings reveal a previously underexplored PCET mechanism facilitated by electron–proton relay between distinct phases, offering new design principles for interfacial redox catalysis.

2. Experimental and methods

2.1. Chemicals and Reagents

Bis (triphenylphosphoranylidene) ammonium chloride (BACl, 98%), lithium tetrakis (pentafluorophenyl)borate ethyl etherate (LiTB), tetracyanoquinodimethane (TCNQ, 98%), and lithium chloride (LiCl, >99%) were obtained from Sigma-Aldrich. Additional reagents, including 1,2-dichloroethane (DCE), 2-hydroxy-3-methoxybenzaldehyde, and hydrochloric acid (37%), were purchased from Merck.

The synthesis of bis (triphenylphosphoranylidene) ammonium tetrakis (pentafluorophenyl)borate (BATB) was carried out via a metathesis reaction between equimolar amounts of BACl and LiTB in a methanol/water mixture (2:1 v/v), followed by recrystallization from acetone.

2.2. Electrochemical Measurements

Electrochemical analysis of the oxygen reduction reaction (ORR) at the water/1,2-dichloroethane (DCE) interface was performed using a four-electrode system. Cyclic voltammetry (CV) measurements were carried out with a PGSTAT 101 micropotentiostat (Eco-Chemie). The setup included two platinum working electrodes, each placed separately in the aqueous and organic phases, along with two Ag/AgCl reference electrodes, one in each phase, to monitor the interfacial potential. Current was passed between the platinum electrodes, while the reference electrodes connected the aqueous and organic compartments.

The electrolyte compositions are detailed in Scheme 1. The Galvani potential difference (Δ_owφ) was calculated based on the reversible half-wave potential of the tetramethylammonium (TMA^+) cation, taken as 0.16 V [30]. All measurements were performed at room temperature (24 ± 1 °C).

2.3. Computational details

To validate the electronic structure calculations, the Hartree-Fock (HF) method was employed using Spartan'10 software. The HF method approximates the wave function and energy of a quantum system by assuming that the multi-electron wave function can be represented by a single Slater determinant of spin orbitals. It uses a self-consistent field approach, where electron-electron repulsion is treated in an averaged mean-field manner. Calculations were performed at three different levels of theory: HF/3-21G, HF/6-31G*, and HF/6-31G**, which differ in the size and quality of their basis sets.

These calculations provided comparative data to assess electronic properties as well as the PA, GB, and aqueous-phase acidity (pKa) of TCNQ at potential proton acceptor sites.

The PA was calculated as the negative of the enthalpy change for the gas-phase protonation reactions, as described by Eqs. (1) and (2).

$$TCNQ(g) + H^+(g) \rightarrow HTCNQ^+(g) \quad (1)$$

$$TCNQ(g) + H_3O^+(g) \rightarrow HTCNQ^+(g) + H_2O(g) \quad (2)$$

Similarly, the gas-phase basicity (GB) corresponds to the negative Gibbs free energy change for the same reactions.

To assess the aqueous acidity (pKa) of the conjugate acid $HTCNQ^+$ at 298.15 K, Eq. (3) was applied. [8, 9, 11, 13].

$$pKa = 1.752\times10^{-4}\ \Delta G^0dep \quad (3)$$

To obtain ΔG°dep, a thermodynamic cycle was constructed, and this value was calculated using a combination of equations involving ΔG°(4) and ΔG°(5). These intermediate free energy terms were derived from specific reactions defined in equations (4) and (5), respectively. ΔG°(4) was further expressed in equation (7).

All calculations were performed under standard conditions (298.15 K and 1 atm). This computational framework provides a detailed understanding of the acid-base behavior of TCNQ, which is essential for its role as an ionophore in the ORR at the interface. Immiscible liquid-liquid interfaces:

$$HTCNQ^+ + H_2O \rightarrow H_3O^+ + TCNQ \quad (4)$$

$$H_3O^+ + H_2O \rightarrow H_3O^+ + H_2O \quad (5)$$

$$\Delta G^0dep = \Delta G^0(5) + \Delta G^0(4) \quad (6)$$

$$\Delta G^0(4) = \Delta G^0g(4) + \Delta G^0aq(4) \quad (7)$$

3. Results and discussion

3.1. Quantum-chemical and electrochemical elucidation of TCNQ as an interfacial electron mediator

The interfacial ORR between ITIES presents unique mechanistic challenges due to phase separation and limited ion transport.

10.57647/ijc.2026.1601.08

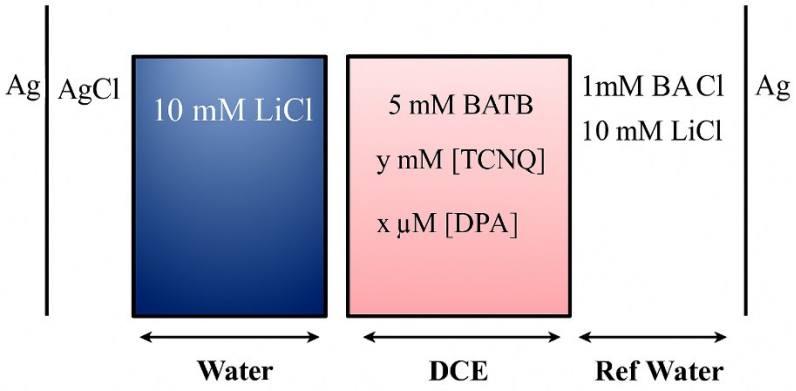

Scheme 1. The composition of the electrochemical cell, which was used in this study

Within this context, the electron-deficient organic molecule TCNQ is a promising redox mediator because of its highly conjugated π-system and four electron-withdrawing cyano groups (–CN) (Fig. 1). TCNQ's electronic structure allows it to accept electrons easily, facilitating redox mediation at the interface. To elucidate TCNQ's dual role as both a proton shuttle and electron acceptor, the study combined quantum chemical calculations with electrochemical characterization under biphasic conditions to provide insights into its cooperative function in the ORR.

The proton affinity (PA) and gas-phase basicity (GB) of the mono- and di-protonated forms of TCNQ were calculated using the Hartree–Fock method with several basis sets (HF/3-21G, HF/6-31G*, and HF/6-31G**) to evaluate its proton-carrying capability (see Table 2a). In addition, the same quantities were computed at the DFT/B3LYP level of theory using the 6-31G**, 6-31+G*, 6-31+G**, and 6-31++G** basis sets, as reported in Table 2b.

The mono-protonated form (TCNQ–H^+) exhibited a positive but modest PA, indicating that single protonation is thermodynamically feasible. In contrast, the di-protonated form (TCNQ–H_2^{2+}) showed negative PA and GB values, suggesting that its formation is thermodynamically unfavorable under the studied conditions. These calculations align with standard computational approaches where proton affinity is derived from changes in electronic energy and zero-point vibrational energies, confirming the limited protonation capacity of TCNQ beyond the mono-protonated state.

This behavior reflects a key electronic characteristic of π-conjugated acceptors like TCNQ: the initial protonation significantly alters the electron density distribution. This perturbation deactivates other potential basic sites through charge delocalization and electrostatic repulsion, limiting further protonation. As a result, multi-protonation of TCNQ is both sterically and electronically hindered, especially in protic or polar environments. This phenomenon arises from the proton-induced reorganization of electronic levels and the formation of electrostatic interactions that stabilize the mono-protonated form while disfavoring additional proton uptake. These effects are consistent with observed reductions in electronic gaps and charge redistribution upon protonation in similar conjugated systems [31].

Further insights were obtained from solution-phase thermodynamics by calculating standard Gibbs free energies (ΔG°) and aqueous pKa values, summarized in Tables 3a and 3b. The computed pKa values for both the mono-protonated (TCNQ–H^+) and di-protonated (TCNQ–H_2^{2+}) forms indicate that TCNQ acts as an extremely weak Brønsted base in aqueous solution. This result aligns with molecular electrostatic potential (MEP) maps (Fig. 2), which reveal localized electron density around the nitrile (–CN) groups but not enough to favor protonation under aqueous conditions. These findings further support TCNQ's limited basicity and protonation propensity in water, consistent with its behavior as a redox mediator rather than a strong proton acceptor.

TCNQ may transiently act as a proton carrier in nonpolar environments, but its contribution to proton-coupled electron transfer (PCET) in aqueous oxygen reduction reaction (ORR) is likely minimal due to its weak proton affinity. In contrast, TCNQ exhibits exceptional electron-accepting ability, characterized by its high electron affinity (EA). Both theoretical and experimental studies, including advanced density functional theory (DFT) and coupled-cluster calculations, consistently show strong agreement with empirical data. The experimentally measured EA of TCNQ is 3.383 ± 0.001 eV (27,289 ± 8 cm^{-1}), which is significantly higher than earlier reported values around 2.8 ± 0.1 eV. This high EA underpins TCNQ's effectiveness as a robust electron acceptor in redox processes [32] , confirming its robust oxidative capacity [33]. Electrochemical studies further confirm TCNQ's electron-accepting function.

Cyclic voltammetry (CV) of TCNQ in 1,2-dichloroethane (DCE) with tetrabutylammonium perchlorate as the supporting electrolyte shows two distinct, reversible redox peaks at approximately –0.25 V and +0.38 V versus Ag/AgCl (Fig. 3).

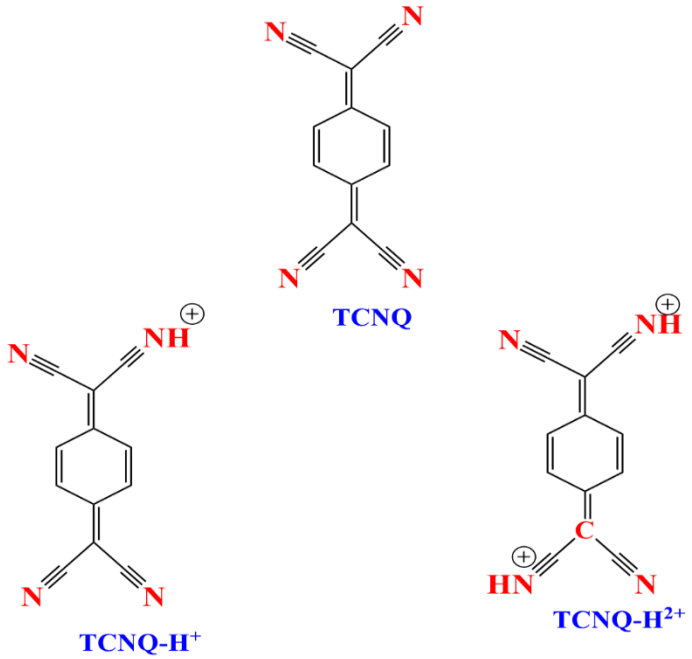

Figure 1. The structure of TCNQ and positions of receiving protons in it

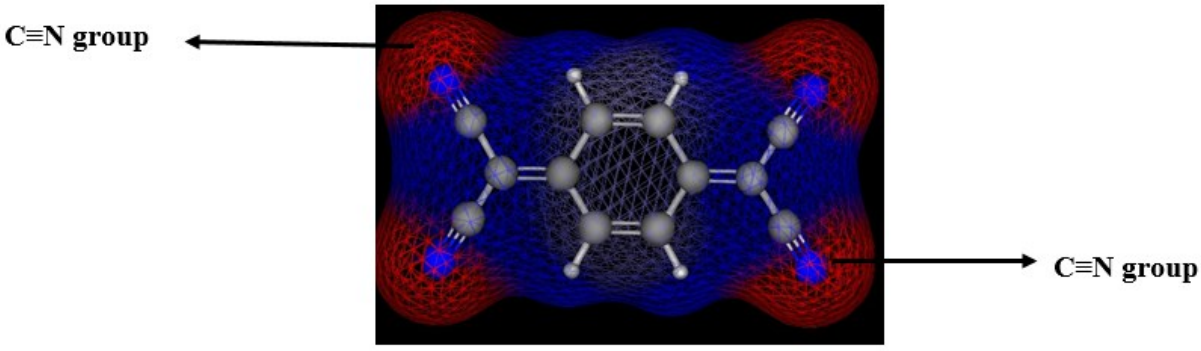

Figure 2. Map of charge for TCNQ

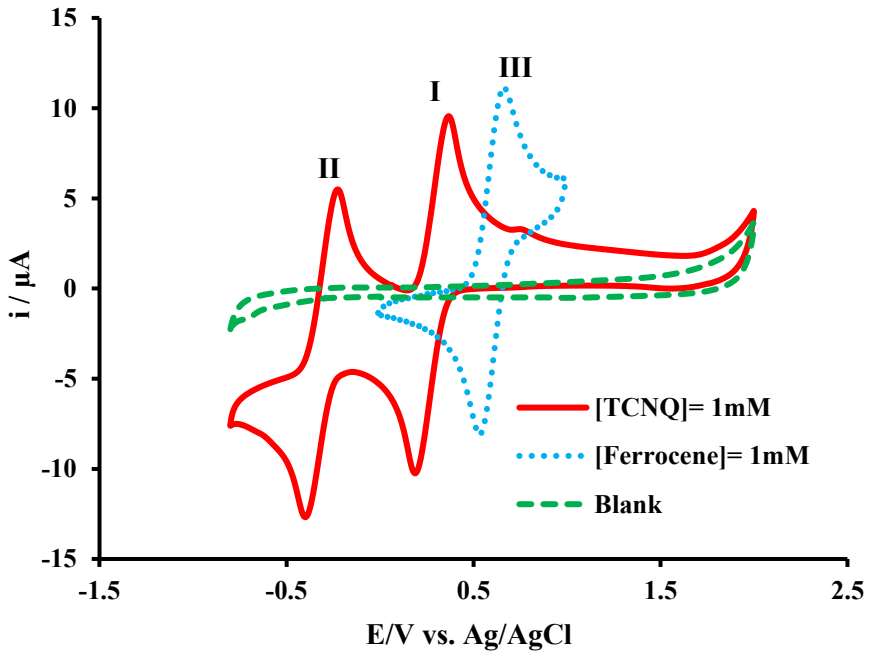

Figure 3. yclic voltammetry (CV) of TCNQ (1 mM) and ferrocene (Fc, 1 mM) was conducted in 1,2-dichloroethane (DCE) containing 0.1 M tetrabutylammonium perchlorate as the supporting electrolyte. A glassy carbon electrode was used as the working electrode, a platinum wire as the counter electrode, and an Ag/AgCl electrode as the reference electrode. The CV measurements were recorded at a scan rate of 0.1 V/s

10.57647/ijc.2026.1601.08

Table 1. Electron transfer rate constants and reproducibility of voltammetric peaks

Peak Number	The electron transfer rate constant (k_0) (cm/s)	%RSD
I	7.6×10^{-3}	5%
II	7.3×10^{-3}	4%
III	1.5×10^{-1}	2%

Table 2a) PA and GB of TCNQ in kJ/mol in the gas phase at room temperatures calculated at the HF /3-21G, 6-31G*, 6-31G** levels of theory

Species	PA/kJmol^{-1}			GB/kJmol^{-1}		
	3-21G	6-31G*	6-31G**	3-21G	6-31G*	6-31G**
TCNQ-H$^+$	16.17	68.32	63.94	16.90	70.36	52.34
TCNQ-H^{2+}	-256.91	-196.71	-206.58	-256.32	-195.86	-205.86

Table 2b) PA and GB of TCNQ in kJ/mol in the gas phase at room temperatures calculated at the DFT/B3LYP/ /6-31G**, 6-31+G*, 6-31+G**, 6-31++G** levels of theory

Species	PA/kJmol^{-1}				GB/kJmol^{-1}			
	6-31G**	6-31+G*	6-31+G**	6-31++G**	6-31G**	6-31+G*	6-31+G**	6-31++G**
TCNQ-H$^+$	84.99	94.67	92.71	92.59	71.44	95.23	93.80	93.68
TCNQ-H^{2+}	-205.67	-184.67	-184.57	-187.02	-343.08	-185.94	-186.90	-187.02

Table 3a) The standard Gibbs free energies and pKa of TCNQ and its conjugate acids in water at room temperatures calculated at the HF /3-21G, 6-31G*, 6-31G** levels of theory

Species	ΔG^0/kJmol^{-1}			pKa		
	3-21G	6-31G*	6-31G**	3-21G	6-31G*	6-31G**
TCNQ	4.45	-27.41	-30.24	-	-	-
TCNQ-H$^+$	-242.28	-285.08	-284.19	23.52	12.06	17.56
TCNQ-H^{2+}	-751.93	-792.75	-793.13	25.33	14.90	18.14

Table 3b) The standard Gibbs free energies and pKa of TCNQ and its conjugate acids in water at room temperatures calculated at the DFT/B3LYP/ /6-31G*, 6-31G**, 6-31+G*levels of theory

Species	ΔG^0/kJmol^{-1}			pKa		
	6-31G*	6-31G**	6-31+G*	6-31G*	6-31G**	6-31+G*
TCNQ	-40.20	-43.303	-45.02			
TCNQ-H$^+$	-252.30	-267.09	-284.19	17.85	13.56	18.06
TCNQ-H^{2+}	-791.93	-782.75	-753.13	20.01	16.80	20.34

These peaks correspond to the stepwise one-electron reductions forming the TCNQ radical anion ($TCNQ^-$) and the dianion ($TCNQ^{2-}$), respectively. The reversible nature of these peaks indicates stable redox cycling and supports TCNQ's role as a robust redox mediator in organic media. Similar CV profiles have been reported in various studies, confirming these characteristic redox transitions for TCNQ species in nonaqueous solvents [34, 35]. The electrochemical data show that the reference redox couple of ferrocene (Fc/Fc^+) at +0.6 V vs Ag/AgCl validates the internal potential calibration and emphasizes the redox accessibility of TCNQ. The dual redox behavior of TCNQ, with reversible reductions forming $TCNQ^-$ and $TCNQ^{2-}$, establishes it as a functional molecular electron sink, optimally suited for interfacial redox mediation where electron transfer must cross hydrophobic/hydrophilic boundaries. This scenario is central to biphasic ORR catalysis.The electron transfer rate constant (k_0) for peak number I was calculated using Nicholson's method based on the peak potential separation (ΔEp) observed in the cyclic voltammetry data [36]. For ΔEp = 0.15 V, the dimensionless kinetic parameter ψ is approximately 1 according to Nicholson's tables.

Using the relation

$k_0 = \psi \times (\pi\, D\, n\, F / R\, T)^{1/2} \times v^{1/2}$

and the experimental parameters:

Diffusion coefficient, $D = 4.75 \times 10^{-6}$ cm²/s

Number of electrons transferred, n = 1

Temperature, T = 298 K

Faraday constant, F = 96485 C/mol Gas constant, R = 8.314 J/(mol K) Scan rate, v = 0.1 V/s

10.57647/ijc.2026.1601.08

The calculated electron transfer rate constant is approximately k_0 = 0.0076 cm/s. This value corresponds to moderately slow electron transfer kinetics, consistent with the observed ΔEp. The results obtained for the electron transfer rate constant and the relative standard deviation (RSD) of the voltammetric peaks observed in Fig. 3 are presented in Table 1. The table summarizes the electron transfer rate constants (k_0) and the relative standard deviations (%RSD) associated with the voltammetric peaks observed in the experiments. Peak I and II show similar rate constants around 7.3×10^{-3} and 7.6×10^{-3} cm/s with %RSD values of 5% and 4%, indicating good reproducibility for these peaks. Peak III demonstrates a significantly higher rate constant of 1.5×10^{-1} cm/s and an excellent reproducibility with %RSD of 2%. These results reflect consistent electron transfer kinetics and reliable measurement precision across the different electrochemical processes analyzed.

The electron transfer rate constants for ORR in this study range from ~7×10^{-3} to 1.5×10^{-1} cm s^{-1}, matching or exceeding values for efficient molecular and heterogeneous catalysts. For comparison, Fe/N/C and Pt/aerogel-NTO catalysts and certain metal-organic frameworks typically exhibit rate constants of 10^{-3} to 10^{-2} cm s^{-1}, confirming comparable effective electron transfer kinetics. [37, 38].

Unlike many mediators, which lack the necessary redox flexibility or stability, TCNQ uniquely combines electronic tunability, chemical robustness, and amphiphilic redox characteristics, making it particularly effective for interfacial mediation in such systems. The stability and reversibility of its multi-electron transfer, coupled with a redox potential appropriately positioned relative to ferrocene, confer TCNQ with distinct advantages in redox catalysis at liquid–liquid interfaces [39, 40].

3.2. Modulation of interfacial electron–proton coupling by dipyridylamine: synergistic enhancement of TCNQ-mediated ORR

To explore the potential synergy between the electron acceptor TCNQ and the proton donor 2,2′-dipyridylamine (DPA) at the polarized water–1,2-dichloroethane (DCE) interface, cyclic voltammetry experiments were conducted under acidic conditions (pH = 2). The impact of varying DPA concentration on the interfacial redox response of TCNQ was investigated. Figure 4 shows the cyclic voltammograms of the first scan recorded at the ITIES using the electrochemical cell setup described in Scheme 1. These experiments probe how increasing proton donor availability influences the PCET behavior of TCNQ at the liquid–liquid interface, providing insight into the cooperative catalytic mechanism under biphasic conditions. The electrochemical stability window in this system is defined by the intrinsic hydrophilicity of Li^+ and Cl^- ions in the aqueous phase and the lipophilicity of BA^+ ions in the organic phase. The negative potential limit is set by the onset of chloride ion (Cl^-) transfer from the aqueous into the organic phase, while the positive potential boundary is constrained by the migration of protons (H^+) and lithium ions (Li^+) into the organic DCE phase. These ion transfer thresholds establish a thermodynamically bounded potential range that permits the investigation of interfacial redox processes without interference from bulk solvent decomposition or unwanted ion crossover. This well-defined potential window ensures electrochemical stability, thereby enabling accurate and reproducible measurements of redox reactions at the liquid–liquid interface. [41].

Upon addition of 5.0 mM TCNQ to the organic phase, a distinct redox couple appears at the polarized water–1,2-dichloroethane (DCE) interface, confirming interfacial redox activity attributed solely to TCNQ. This signal is absent in the "Blank" voltammogram, lacking both TCNQ and DPA, confirming the role of TCNQ in mediating electron transfer at the interface. The observed redox peaks align with theoretical data showing TCNQ's strong electron-accepting character but weak proton affinity in aqueous media, supporting an interfacial electron transfer (ET) mechanism dominating over PCET when no external proton donor is present. This highlights TCNQ's role as a molecular electron sink, effectively facilitating electron transfer across the liquid–liquid interface, consistent with previous electrochemical and spectroscopic studies at ITIES [40]. Cyclic voltammetry at the water/1,2-dichloroethane interface yielded a diffusion coefficient of 2.18×10^{-14} cm^2/s and an electron transfer rate constant of 1.16×10^{-5} cm/s for TCNQ, calculated via Nicholson's method. These measurements showed excellent repeatability (~9%), confirming reliable kinetics. The results indicate slow kinetics and limited ion diffusion typical of immiscible liquid-liquid interfaces due to complex transport characteristics. Overall, these data provide valuable insights into interfacial electrochemical processes and ion transfer in biphasic systems.The ion transfer rate constant ($k^0 \approx 10^{-5}$ cm s^{-1}) determined in this study for proton shuttling during TCNQ-DPA mediated ORR at the polarized water|1,2-dichloroethane (DCE) interface, derived via Nicholson's method from cyclic voltammetry peak separations (ΔE_p analysis), resides within the canonical range for both simple and facilitated ion transfers across ITIES. For benchmark unassisted transfers, tetraalkylammonium cations (TAA^+) like tetraethylammonium (TEA^+) exhibit faster k^0 = 0.018–0.64 cm s^{-1} [42] owing to amphiphilic solvation minimizing hydration shells, whereas hydrophilic inorganic anions (e.g., Cl^-, F^-) or alkali cations (e.g., Na^+) decelerate to 10^{-6}–10^{-5} cm s^{-1} [43], precisely bracketing our DPA-facilitated proton relay where diffusion

10.57647/ijc.2026.1601.08

coefficients ($D = 2.18\times10^{-14}$ cm² s⁻¹) impose the primary limitation. Facilitated processes further contextualize these results: phospholipid monolayers or ion-pairing agents (e.g., H_3O^+-$TPFB^-$) elevate rates to ~10^{-5}–10^{-4} cm s⁻¹ [44] by stabilizing transition states ($\Delta G^*_{TS} \approx 6$–$10$ kcal mol⁻¹ reduction via ion-pairing), as seen for $IrCl_6^{2-}$ transfers [45], yet our system achieves comparable PCET synchronization, doubling H_2O_2 yield from 38±4% to 78±8% without exogenous facilitators, highlighting DPA's bidentate amine efficacy in mitigating proton-deficient organic phases. Solvent viscosity modulates this kinetics, with higher-η media like o-nitrophenyl octyl ether (o-NPOE) yielding $k^0 < 10^{-6}$ cm s⁻¹ ($\eta \propto 1/\sqrt{D}$ scaling), whereas DCE's lower viscosity ($\eta = 1.3$ cP) supports our observed rates.

Micro-ITIES or nanopipette geometries artifactually accelerate apparent k^0 (e.g., 0.21–0.32 cm s⁻¹ for TBA^+ in natural oils) [46] due to enhanced mass transport, but macroscopic flat interfaces like ours align with bulk literature benchmarks. The addition of 2,2′-dipyridylamine (DPA) to the aqueous phase at concentrations of 2.4×10^{-5} M and 5.6×10^{-5} M (green and blue curves, respectively) results in a significant and concentration-dependent increase in both anodic and cathodic peak currents in cyclic voltammetry measurements. This enhancement indicates that DPA markedly modulates the interfacial redox kinetics of TCNQ at the polarized water–DCE interface. Structurally, DPA is a bidentate heteroaromatic amine with two pyridyl rings and a central secondary amine proton donor site, which enables noncovalent interactions such as hydrogen bonding, π–π stacking, and proton transfer with reduced TCNQ species like $TCNQ^-$ or $TCNQ^{2-}$. These transient interactions at the interface help stabilize charge-separated states and alter the free energy landscape of TCNQ redox transitions, facilitating improved PCET kinetics [47]. DPA is proposed to function as a proton-shuttling co-mediator, facilitating interfacial PCET by donating protons to the reduced TCNQ species. This proton donation can reduce the reorganization energy and lower the activation barrier for electron transfer at the interface, thereby accelerating the redox reaction. The observed increase in peak current with higher DPA concentration supports this mechanism, suggesting that the redox conversion rate is influenced not only by TCNQ diffusion but also by the availability and reactivity of proton donors like DPA at the interface. These insights align with current understanding of redox hopping and proton shuttle mechanisms, where molecular mediators and proton donors interact to optimize electron and proton transfer kinetics [48]. The biphasic interplay of ET and PT mediated by small molecules like DPA introduces a novel mechanistic dimension for regulating interfacial electron transfer in phase-separated, heterogeneous media. By effectively decoupling the electronic and protonic components of the redox event, this system mirrors aspects of biological electron transport chains, where proton relays are crucial for ensuring directionality and efficiency of electron flow. Consequently, the TCNQ–DPA system serves as a functional model for phase-separated PCET processes, providing new insights and opportunities for designing biphasic electrocatalysts and redox mediators with enhanced catalytic performance and molecular-level tunability. This approach leverages dynamic proton shuttling and electron mediation to optimize interfacial charge transfer in non-homogeneous environments [48]. The ion transfer rate constant at the liquid-liquid interface is ~10^{-6} cm s⁻¹, consistent with typical values for immiscible electrolyte interfaces (10^{-6} to 10^{-5} cm s⁻¹). This slow rate reflects the complex transport environment at the interface and underscores ion-transfer limitations affecting overall catalytic efficiency [49]. The notable enhancement in proton-coupled electron transfer and H_2O_2 production confirms a highly synergistic system. This aligns with recent studies emphasizing proton shuttles' crucial role in regulating ORR kinetics and selectivity [50]. These comparisons confirm the kinetic robustness and competitive performance of the TCNQ-DPA system for interfacial catalysis. They demonstrate their potential as an efficient catalyst in biphasic energy conversion applications. To investigate the interfacial reduction of molecular oxygen through a synergistic mechanism involving electron donation by TCNQ and proton shuttling catalyzed by DPA, we employed a biphasic Galvani cell configuration (also referred to as a shake-flask system) [51]. This setup leverages the distinct physicochemical properties of two immiscible liquid phases to spatially separate the redox components while enabling controlled interfacial coupling. The electrochemical cell used in the study consisted of two immiscible liquid phases: an upper aqueous phase and a lower organic phase composed of DCE. The aqueous phase contained 5 mM lithium tetraborate (LiTB) and 10 mM hydrochloric acid (HCl), while the organic phase comprised 5 mM bis (triphenylphosphoranylidene) ammonium tetraborate (BATB), 5 mM TCNQ, and 100 µM DPA. This biphasic configuration created a stable liquid-liquid interface necessary for studying interfacial redox reactions. The system allowed selective positioning of reactants in their preferred solvents, facilitating electron and proton transfer processes across the hydrophilic-hydrophobic boundary under polarizable conditions. Such biphasic electrochemical cells are widely used for investigating charge transfer and catalytic processes at immiscible electrolyte interfaces, offering a robust platform for mechanistic studies in phase-separated environments (Scheme 2) [52].

10.57647/ijc.2026.1601.08

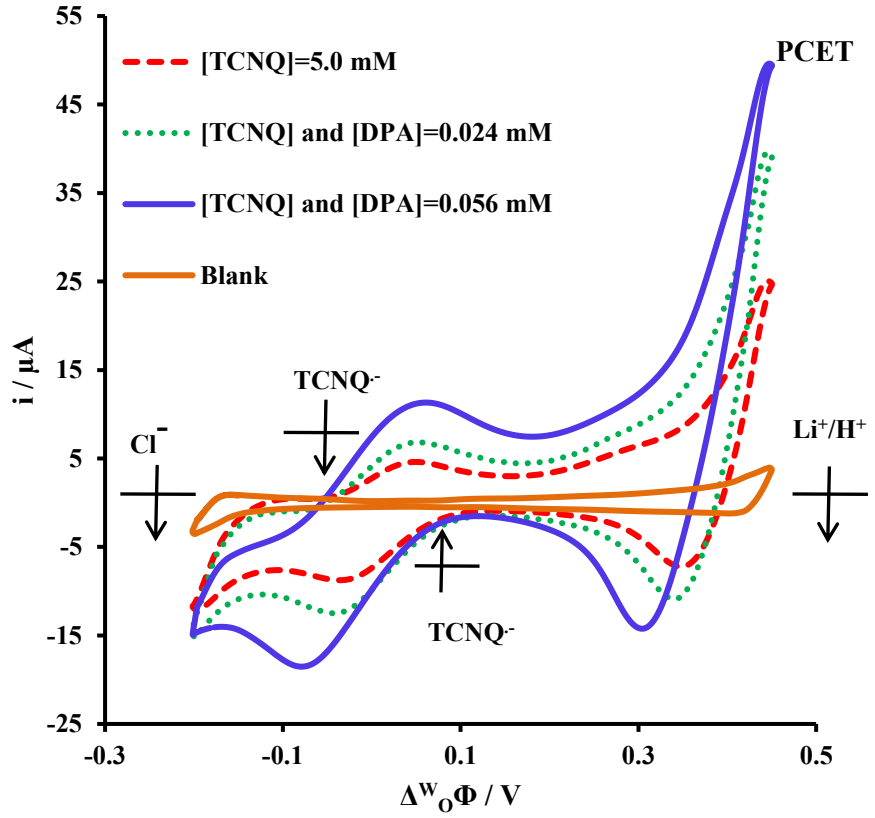

Figure 4. Cyclic voltammetry at a water-DCE interface with the cell illustrated in Scheme 1 in the presence of y=5 mM and different concentrations of x at pH 2 and scan rate 0.05 V s^{-1}

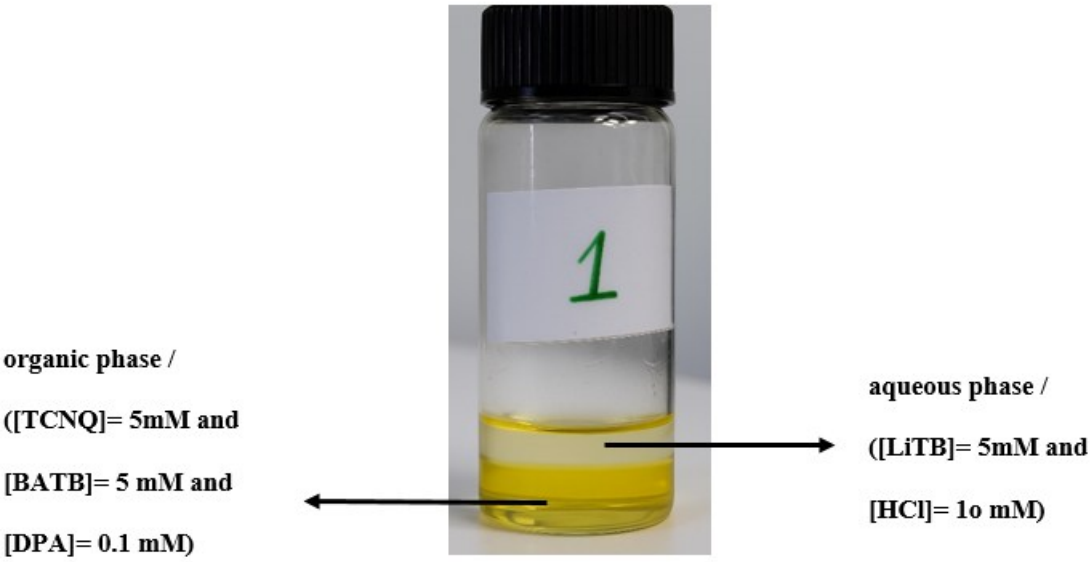

Scheme 2. Photographs of the two-phase reactions, the aqueous phase (top layer) is identical and contains 5 mM LiTB and 10 mM HCl. The organic phase composition is as follows: 5 mM TCNQ, 5 mM BATB, and 100 µM DPA

A Galvani potential difference of 0.54 V was established across the water–1,2-dichloroethane (DCE) interface by distribution of the supporting electrolytes LiTB and BATB, both of which incorporate the tetraarylborate (TB^-) anion as a lipophilic common ion. This engineered interfacial potential difference is crucial for driving the thermodynamically uphill proton transfer from the aqueous phase into the organic phase. In this system, DPA acts as a catalytic proton shuttle enabling proton relay across the immiscible interface via dynamic hydrogen bonding and acid–base interactions. The presence of DPA near the interface facilitates PCET, synchronizing proton translocation with the reduction of molecular oxygen by TCNQ. This coordination effectively lowers the kinetic barrier and enhances biphasic ORR efficiency.

10.57647/ijc.2026.1601.08

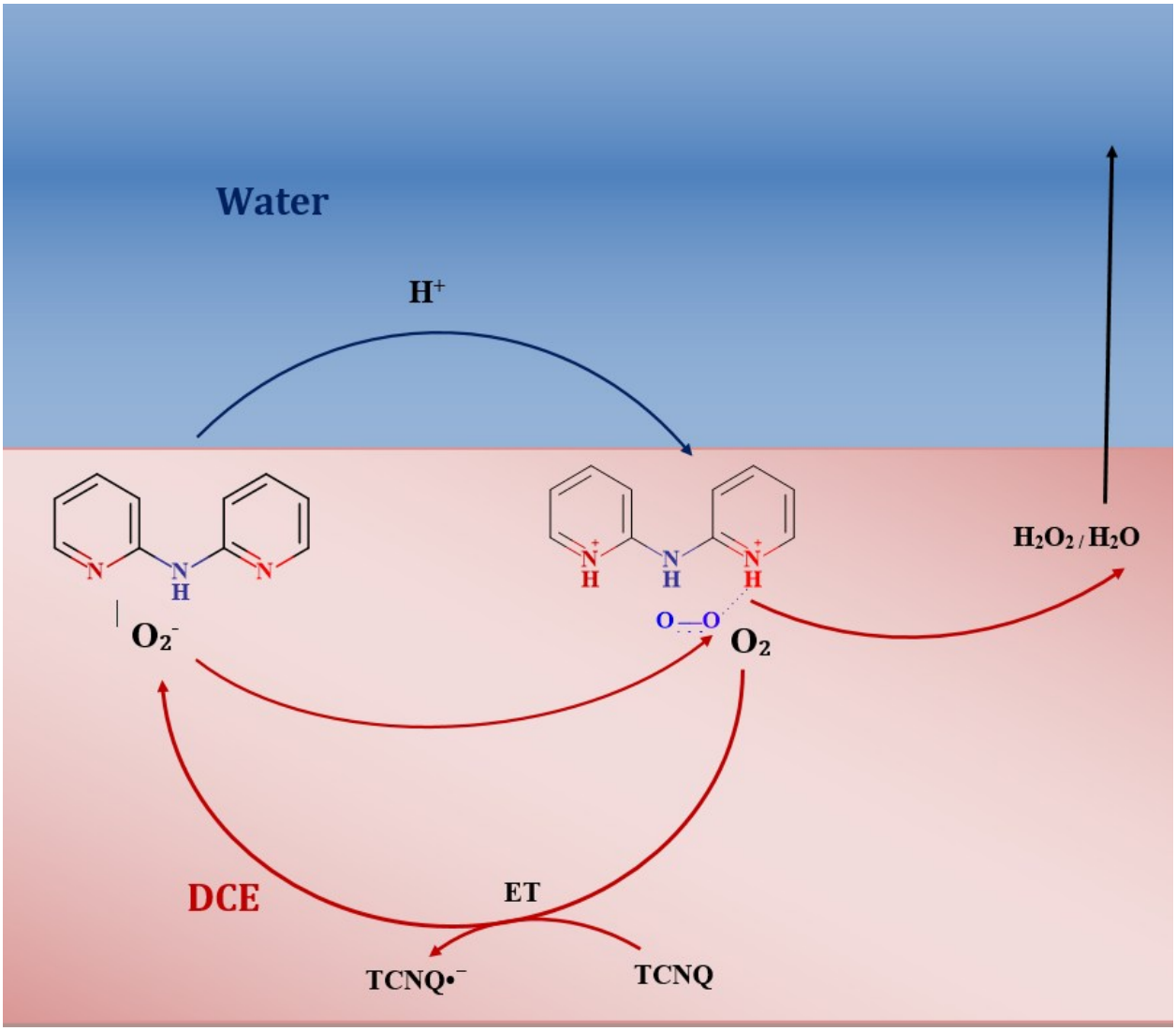

Scheme 3. Mechanism of O_2 reduction with TCNQ catalyzed by DPA

By spatially decoupling the proton donor (DPA in aqueous phase) and electron donor (TCNQ in organic phase), the system introduces a mechanistic advancement in interfacial electrocatalysis. It enables independent tuning of each phase, providing a platform for the rational design of next-generation biphasic redox systems with optimized catalytic performance. This state-of-the-art approach leverages the partitioning of lipophilic and hydrophilic ions to control the Galvani potential difference, promoting selective charge transfer processes at the interface [53].

To investigate hydrogen peroxide (H_2O_2) formation as a two-electron product of oxygen reduction, an iodometric assay was employed. After 40 minutes of stirring the biphasic system, potassium iodide (KI) was added to the aqueous phase to a final concentration of 0.2 M. In this assay, H_2O_2 oxidizes iodide ions (I^-) to form triiodide (I_3^-), which exhibits characteristic UV-Vis absorption peaks at 290 nm and 355 nm. According to Figure 5, the interfacial system containing only TCNQ produced negligible H_2O_2, indicating limited efficiency of electron transfer alone in oxygen reduction. In contrast, when both TCNQ and DPA were present, a substantial increase in H_2O_2 formation was observed, highlighting DPA's critical role in proton transfer and completing the reduction process. According to the study's detailed findings (Fig. 5b), H_2O_2 production yield was significantly enhanced by DPA as a catalyst. TCNQ alone yielded only ~38% (4 mM) H_2O_2, indicating modest ORR efficiency. With DPA added as a proton shuttle alongside TCNQ, the yield increased substantially to ~78% (8 mM) substantially. This marked improvement reflects a synergistic effect: TCNQ mediates electron transfer while DPA facilitates proton transport across the water-organic interface, enabling efficient PCET. This result strongly supports a proton-coupled electron transfer (PCET) mechanism facilitated by the synergistic action of TCNQ and DPA at the liquid–liquid interface. The iodometric method is a widely recognized, reliable, and sensitive spectrophotometric approach for quantifying H_2O_2 through its oxidation of iodide to colored triiodide species, enabling straightforward monitoring of reaction progress. The proposed oxygen reduction mechanism at the biphasic interface involving TCNQ and DPA can be summarized in these steps (Scheme 3):

10.57647/ijc.2026.1601.08

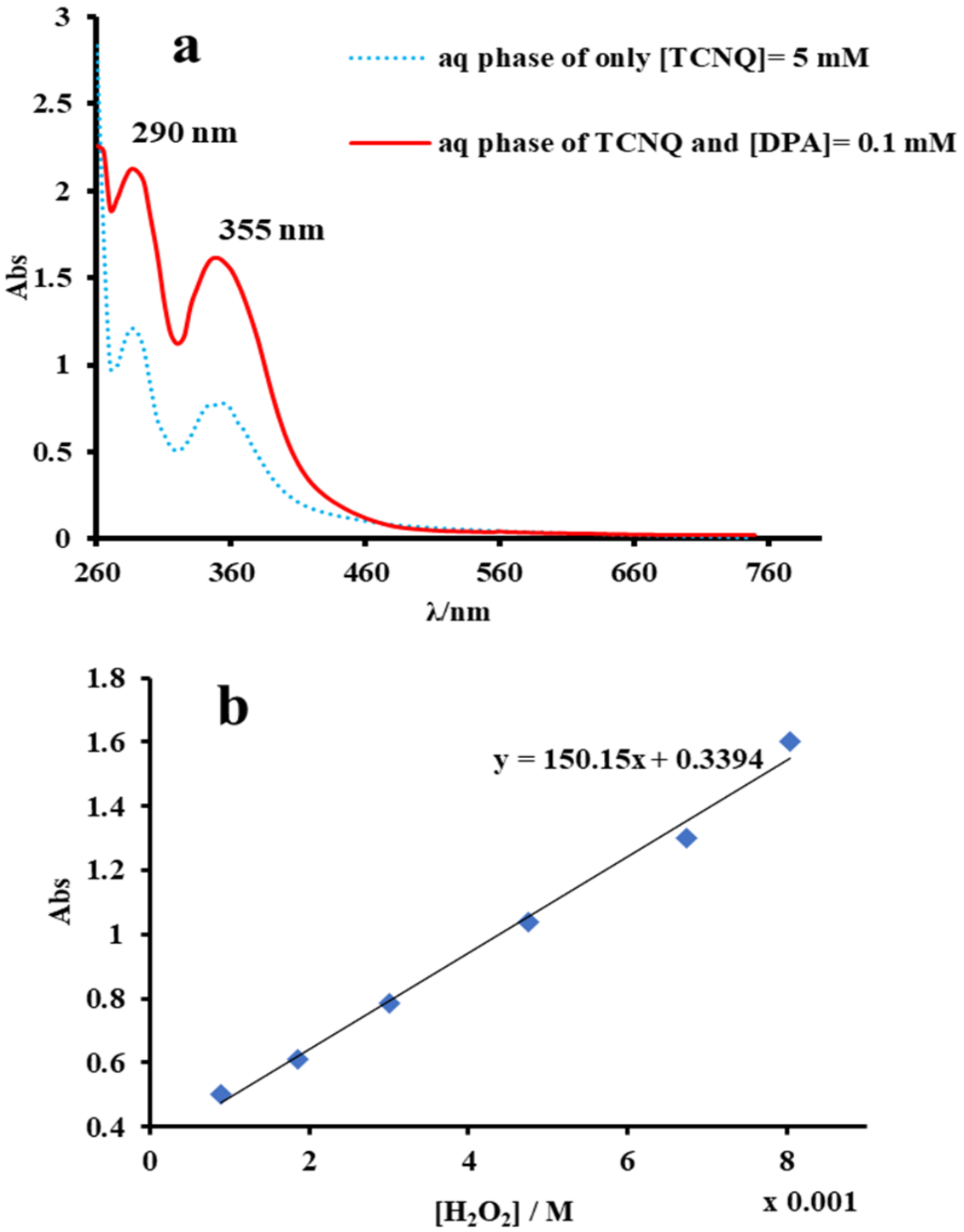

Figure 5. a) UV-Vis spectra of the aqueous phase, b) Calibration curves of [H_2O_2]

1) TCNQ in the organic phase (o) undergoes one-electron reduction to form the radical anion TCNQ-$^{-}$ as it donates an electron at the interface:

$$TCNQ\ (o) \rightarrow TCNQ^{\bullet -}\ (o) + e^{-} \quad (8)$$

This step highlights TCNQ acting as a weak electron donor to initiate reduction.

2) The dissolved oxygen (O_2) in the aqueous phase (w) accepts the electron to generate the superoxide radical anion:

$$O_2\text{-}^{-}{:}O_2(o) + e^{-} \rightarrow O_2^{\bullet -}\ (o) \quad (9)$$

This formation of superoxide is typical in oxygen reduction reactions and represents the key reactive intermediate.

3) A proton donor, such as protonated DPA ($DPAH^{+}$), provides a proton to convert superoxide into the hydroperoxyl radical:

$$HO_2\text{-}:O_2^{\bullet -}(o) + DPAH^{+}(o) \rightarrow HO_2^{\bullet}(w) + DPA\ (o) \quad (10)$$

This proton transfer step, facilitated by DPA at the interface is critical in progressing the reduction sequence by stabilizing charge-separated species and enabling PCET.This mechanism explains how TCNQ and DPA

10.57647/ijc.2026.1601.08

cooperate at the immiscible electrolyte interface to achieve efficient oxygen reduction through synergistic electron donation and proton shuttling, consistent with computational and electrochemical data showing minimal hydrogen peroxide byproduct and enhanced PCET facilitated by molecular mediators.

3.3. Unified Mechanistic Interpretation of the Interfacial ORR Mediated by TCNQ and DPA

To provide a clearer and more coherent presentation, the mechanistic explanation of the interfacial ORR has been consolidated into a single subsection. This integrates electrochemical observations, thermodynamic trends, and quantum-chemical calculations into a unified description consistent with recent literature on interfacial PCET systems. At the polarized aqueous/organic boundary, TCNQ serves as the primary electron mediator. Cyclic voltammetry results demonstrate its stepwise, reversible reduction to $TCNQ^{-}$ and $TCNQ^{2-}$, confirming stable redox cycling within the organic phase [35, 40]. The experimentally low reduction potentials and high calculated electron affinities confirm TCNQ's strong thermodynamic driving force for interfacial electron transfer to dissolved O_2.

Although quantum-chemical results suggest mono-protonation of TCNQ is theoretically feasible, the calculated proton affinity, gas-phase basicity, and aqueous pKa values demonstrate that TCNQ acts as a weak Brønsted base under aqueous conditions [54, 55]. Therefore, TCNQ primarily functions as an efficient electron donor rather than a significant proton carrier in the aqueous-phase ORR. This limitation is compensated for by DPA, which serves as a mobile proton shuttle that transports protons from the aqueous phase to the interfacial reaction zone. This mechanism aligns with prior studies demonstrating that pyridylamine-based molecules efficiently facilitate proton transport in liquid-liquid electrocatalytic systems [9, 56].

In the presence of DPA, electron transfer from reduced TCNQ species occurs concurrently with proton delivery from the aqueous phase, establishing a cooperative proton-electron relay. This synchronized mechanism minimizes kinetic mismatch and prevents accumulation of partially reduced oxygen intermediates. In this unified mechanism, O_2 near the interface is reduced by $TCNQ^{-}$ or $TCNQ^{2-}$, while proton transfer from DPA completes the PCET steps, stabilizing intermediates and lowering activation barriers. DFT results further confirm that interfacial confinement and solvent reorganization enhance the thermodynamic favorability of ORR transition states [57]. Overall, the combined electrochemical and computational evidence strongly supports a synergistic ORR pathway where TCNQ mediates electron delivery, and DPA supplies protons in a coordinated fashion. This cooperation enables more efficient PCET and offers a promising strategy for designing next-generation biphasic electrocatalytic systems for energy conversion and environmental remediation [57].

4. Conclusion

This study reveals a novel cooperative mechanism for interfacial oxygen reduction reaction (ORR) using tetracyanoquinodimethane (TCNQ) as an electron mediator and dipyridylamine (DPA) as a proton shuttle at the immiscible aqueous-organic interface. Unlike traditional ORR in homogeneous media or on solid electrodes, this biphasic liquid-liquid interface allows independent optimization of proton and electron transfers. Quantum chemical analyses confirm TCNQ's strong electron-accepting ability but limited proton affinity, requiring a proton shuttle like DPA. DPA significantly enhances proton-coupled electron transfer (PCET) efficiency, as shown by improved electrochemical kinetics and higher hydrogen peroxide yields in shake-flask assays, with cyclic voltammetry verifying TCNQ's reversible redox behavior. This dual-mediator system provides a new framework for interfacial catalysis, pairing redox mediators with proton shuttles to optimize biphasic electrocatalysis mimicking biological electron transport chains. It establishes design principles for soft-interface electrocatalysts: combining electron acceptors with compatible proton shuttles boosts efficiency and selectivity for energy conversion, green chemistry, and sensing applications.

Acknowledgments
This work received financial support from Jundi-Shapur University of Technology, Dezful, Iran, which is greatly appreciated.

Declarations
Ethical approval: This study did not involve human participants or animal experiments; therefore, ethical approval was not required.

Consent to participate: Not applicable, as the study did not involve human participants.

Consent to publish: All authors have read and approved the final version of the manuscript and consent to its publication.

Funding Declaration
This research received no specific grant from any funding agency in the public, commercial, or not-for-profit sectors.
Ethics, Consent to Participate, and Consent to Publish declarations: not applicable.

Clinical trial
Our study is not a clinical trial.

Data Availability
The datasets generated during and/or analysed during the current study are available from the corresponding author on reasonable request.

References

[1] C.W. Anson, S.S. Stahl, Chem. Rev. **120** (2020) 3749-3786. https://doi.org/10.1021/acs.chemrev.9b00717

[2] B. Zhang, L. Sun, Chem. Soc. Rev. **48** (2019) 2216-2264. https://doi.org/10.1039/C8CS00897C

[3] M.A. Kamyabi, F. Soleymani-Bonoti, R. Bikas, H. Hosseini-Monfared, N. Arshadi, M. Siczek, T. Lis, Phys. Chem. Chem. Phys. **17** (2015) 32161-32172. https://doi.org/10.1039/C5CP04695E

[4] Giddaerappa, N. Manjunatha, Shantharaja, M. Hojamberdiev, L.K. Sannegowda, ACS Omega. **7** (2022) 14291-14304. https://doi.org/10.1021/acsomega.2c01157

[5] A.C. Kumbara, N. Kousar, L.K. Sannegowda, Journal of Energy Storage. **97** (2024) 112920. https://doi.org/10.1016/j.est.2024.112920

[6] Y. Wang, G.I. Waterhouse, L. Shang, T. Zhang, Ad. Energy Mater. 11 (2021) 2003323. https://doi.org/10.1002/aenm.202003323

[7] D.-W. Wang, D. Su, Energy Environ. Sci. 7 (2014) 576-591. https://doi.org/10.1039/C3EE43463J

[8] M.A. Kamyabi, F. Amirkhani, R. Bikas, F. Soleymani-Bonoti, J. Mol. Struct. 1228 (2021) 129693. https://doi.org/10.1016/j.molstruc.2020.129693

[9] F. Soleymani-Bonoti, J. Mol. Model. **26** (2020) 350. https://doi.org/10.1007/s00894-020-04605-z

[10] M.A. Kamyabi, F. Alirezaei, F. Soleymani-Bonoti, R. Bikas, M. Siczek, T. Lis, Appl. Organomet. Chem. **34** (2020) e5833. https://doi.org/10.1002/aoc.583

[11] F. Soleymani-Bonoti, M.A. Kamyabi, N. Arshadi, Comput. Theo. Chem. **1092** (2016) 47-51. https://doi.org/10.1016/j.comptc.2016.07.026

[12] M.A. Kamyabi, F. Soleymani-Bonoti, R. Bikas, H. Hosseini-Monfared, J. Electroanal. Chem. **794** (2017) 235-243. https://doi.org/10.1016/j.jelechem.2017.04.021

[13] F. Soleymani-Bonoti, N. Aminijam, Chem. Phys. **595** (2025) 112710. https://doi.org/10.1016/j.chemphys.2025.112710

[14] I.H. Patir, J. Electroanal. Chem. **685** (2012) 28-32. https://doi.org/10.1016/j.jelechem.2012.09.001

[15] P. Peljo, L. Qiao, L. Murtomki, Ch. Johans, H. H. Girault, K. Kontturi, ChemPhysChem. **14** (2013) 311–314. https://doi.org/10.1002/cphc.201200953

[16] P. Peljo, L. Murtomaki, T. Kallio, H.-J. Xu, M. Meyer, C.P. Gros, J.-M. Barbe, H.H. Girault, K. Laasonen, K. Kontturi, J. Am. Chem. Soc. **134** (2012) 5974-5984. https://doi.org/10.1021/ja3004914

[17] Y. Xuan, X. Huang, B. Su, J. Phys. Chem. C. **119** (2015) 11685-11693. https://doi.org/10.1021/acs.jpcc.5b02131

[18] M. Opallo, K. Dusilo, M. Warczak, J. Kalisz, ChemElectroChem. **9** (2022) e202200513. https://doi.org/10.1002/celc.202200513

[19] E.C. Tse, C.J. Barile, N.A. Kirchschlager, Y. Li, J.P. Gewargis, S.C. Zimmerman, A. Hosseini, A.A. Gewirth, Nat. Mater. **15** (2016) 754-759.

[20] M.A. Kamyabi, F. Soleymani-Bonoti, F. Alirezaei, R. Bikas, N. Noshiranzadeh, M. Emami, M.S. Krawczyk, T. Lis, Appl. Organomet. Chem. **33** (2019) e5214. https://doi.org/10.1002/aoc.5214

[21] M.U. Khan, S. Nadeem, A. Fatima, J. Yaqoob, M. Khalid, F. Abbas, N. Alhokbany, M.R.S.A. Janjua, J. Mol. Liq. **391** (2023) 123258. https://doi.org/10.1016/j.molliq.2023.123258

[22] S. Sarfraz, S. Ali, S.A. Khan, K.H. Shah, S. Amin, M. Mujahid, S. Jamil, M.R.S.A. Janjua, J. Mol. Liq. **285** (2019) 403-407. https://doi.org/10.1016/j.molliq.2019.04.131

[23] S. Naz, G. Bibi, S. Jamil, S. UrRehman, S. Bibi, S. Ali, T. Khan, S.R. Khan, M.R.S.A. Janjua, Chem. Phys. Lett. **802** (2022) 139768. https://doi.org/10.1016/j.cplett.2022.139768

[24] M.R.S.A. Janjua, Z.-M. Su, W. Guan, A. Irfan, S. Muhammad, M. Iqbal, Can. J. Chem. **88** (2010) 434-442. https://doi.org/10.1139/V10-019

[25] S. Shahzadi, M. Akhtar, M. Arshad, M.H. Ijaz, M.R.S.A. Janjua, RSC Adv. **14** (2024) 27575-27607. https://doi.org/10.1039/D4RA05183A

[26] M.R.S.A. Janjua, J. Photochem. Photobiol. A Chem. **444** (2023) 115003. https://doi.org/10.1016/j.jphotochem.2023.115003

[27] M.R.S.A. Janjua, J. Cluster Sci. **28** (2017) 2419-2431.

[28] T. Mubashir, M.H. Tahir, M. Mahmoud, Z. Shafiq, M. Ashraf, I.H. El Azab, Z.M. El-Bahy, M.R.S.A. Janjua, J. Photochem. Photobiol. A Chem. **444** (2023) 114977. https://doi.org/10.1016/j.jphotochem.2023.114977

[29] B. Basha, M. Sulaman, S. Elshahat, H.M. Jafri, Z. Alrowaili, M. Al-Buriahi, M.R.S.A. Janjua, Mater. Sci. Eng. B. **296** (2023) 116618. https://doi.org/10.1016/j.mseb.2023.116618

[30] V.J. Cunnane, D.J. Schiffrin, C. Beltran, G. Geblewicz, T. Solomon, J. Electroanal. Chem. Interfacial Electrochem. **247** (1988) 203-214. https://doi.org/10.1016/0022-0728(88)80141-4

[31] M. Guerrini, E. Delgado Aznar, C. Cocchi, J. Phys. Chem. C. **124** (2020) 27801-27810. https://doi.org/10.1021/acs.jpcc.0c08812

[32] R. Otero, R. Miranda, J.M. Gallego, ACS Omega. **4** (2019) 16906-16915. https://doi.org/10.1021/acsomega.9b02154

[33] B. Milián, R. Pou-Amérigo, R. Viruela, E. Ortí, Chem. Phys. Lett. **391** (2004) 148-151. https://doi.org/10.1016/j.cplett.2004.04.102

10.57647/ijc.2026.1601.08

[34] T.-C. Tseng, C. Urban, Y. Wang, R. Otero, S.L. Tait, M. Alcamí, D. Écija, M. Trelka, J.M. Gallego, N. Lin, Nat. Chem. **2** (2010) 374-379.

[35] A. Atifi, M.D. Ryan, Molecules. **25** (2020) 303. https://doi.org/10.3390/molecules25020303

[36] R.S. Nicholson, Anal. Chem. **37** (1965) 1351-1355. https://doi.org/10.1021/ac60230a016

[37] A. Muthukrishnan, Y. Nabae, J. Phys. Chem. C. **120** (2016) 22515-22525. https://doi.org/10.1021/acs.jpcc.6b07905

[38] C. He, S. Sankarasubramanian, I. Matanovic, P. Atanassov, V. Ramani, ChemSusChem. **12** (2019) 3468-3480. https://doi.org/10.1002/cssc.201900499

[39] L. Ma, P. Hu, H. Jiang, C. Kloc, H. Sun, C. Soci, A.A. Voityuk, M.E. Michel-Beyerle, G.G. Gurzadyan, Sci. Rep. **6** (2016) 28510.

[40] R. Vishwanath, E.W. Nery, M. Jönsson-Niedziółka, Journal of Electroanalytical Chemistry. **854** (2019) 113558. https://doi.org/10.1016/j.jelechem.2019.113558

[41] R. Hausbrand, J. Chem. Phys. **152** (2020). https://doi.org/10.1063/1.5143106

[42] Z. Samec, J. Langmaier, A. Trojánek, E. Samcová, J. MÁLEK, Anal. Sci. **14** (1998) 35-41.

[43] R. Cui, Q. Li, D.E. Gross, X. Meng, B. Li, M. Marquez, R. Yang, J.L. Sessler, Y. Shao, J. Am. Chem. Soc. **130** (2008) 14364-14365. https://doi.org/0.1021/ja806104z

[44] I. Benjamin, J. Phys. Chem. B. **128** (2024) 9613-9618. https://doi.org/10.1021/acs.jpcb.4c04328

[45] J. Zhang, P.R. Unwin, Langmuir. **18** (2002) 2313-2318. https://doi.org/10.1021/la011605z

[46] R. Chen, K. Xu, M. Shen, Electrochim. Acta. **357** (2020) 136788. https://doi.org/10.1016/j.electacta.2020.136788

[47] Y. Cheng, D.J. Schiffrin, Journal of the Chemical Society, Faraday Trans. **90** (1994) 2517-2523. https://doi.org/10.1039/FT9949002517

[48] M. Yan, Z. Bowman, Z.J. Knepp, A. Peterson, L.A. Fredin, A.J. Morris, J. Phys. Chem. Lett. **15** (2024) 11919-11926. https://doi.org/10.1021/acs.jpclett.4c01674

[49] T. Nakamura, K. Ikeda, H. Morinaga, T. Yoshida, Electrochemistry. **92** (2024) 107001-107001

[50] Q. Wang, H. Guesmi, S. Tingry, D. Cornu, Y. Holade, S.D. Minteer, ACS Energy Lett. **7** (2022) 952-957. https://doi.org/10.1021/acsenergylett.2c00181

[51] I. Hatay, B. Su, F. Li, M.A. Méndez, T. Khoury, C.P. Gros, J.-M. Barbe, M. Ersoz, Z. Samec, H.H. Girault, J. Am. Chem. Soc. **131** (2009) 13453-13459. https://doi.org/10.1021/ja904569p

[52] M.R. Serial, M.I. Velasco, E.V. Silletta, F.M. Zanotto, S.A. Dassie, R.H. Acosta. ChemPhysChem **18** (2017) 3469-3477. https://doi.org/10.1002/cphc.201700775

[53] L. Hung, J. Electroanal. Chem. **115** (1980) 159-174. https://doi.org/10.1016/0368-1874(80)80405-9

[54] B. Huang, Q. Gu, X. Tang, D. Lützenkirchen-Hecht, K. Yuan, Y. Chen, Nat. Commun. **15** (2024) 6077.

[55] R. Jono, J.-i. Fujisawa, H. Segawa, K. Yamashita, Phys. Chem. Chem. Phys. **15** (2013) 18584-18588. https://doi.org/10.1039/C3CP52844H

[56] X. Yin, L. Lin, U. Martinez, P. Zelenay, ACS Appl. Energy Mater. **2** (2019) 7272-7278. https://doi.org/10.1021/acsaem.9b01227

[57] Y. Wu, A. Vriza, D. Ozgulbas, R. Vescovi, J. Zhou, Z. Wang, S. Hu, Y. Zhang, Q. Yang, A. Österholm, J. Reynolds, S. Sankaranarayanan, M. Chan, I. Foster, H. Chan, J. Mei, J. Xu, Mater. chem. (2025). https://doi.org/10.26434/chemrxiv-2025-9pqc